中國機械工程學刊第四十二卷第一期第 11~21 頁(民國一百一十年)
Journal of the Chinese Society of Mechanical Engineers, Vol.42, No.1, pp 11~21 (2021)

Derailment Risk Analysis for Railway Vehicles Subjected to Wind Loads

Yung-Chang Cheng*, Chern-Hwa Chen** and Chung-Wei Yeh***

Keywords： heuristic nonlinear creep model, rail irregularity, wind loads, derailment quotient, offload factor, overturn factor.

ABSTRACT

Based on the heuristic nonlinear creep model, this paper presents the nonlinear differential equations of motion for a railway vehicle model running on curved tracks under two-direction rail irregularities and various cross-wind loads. A 31-degree-of-freedom (31-DOF) vehicle model is constructed by including the lateral, vertical, roll and yaw motions for each wheelset and the lateral, vertical, roll, pitch and yaw motions for the bogie frames and the car body. According to the derailment criterion, the derailment quotients, offload factors and overturn factors for a railway vehicle are determined, respectively. From the numerical results, it shows that the derailment quotients, offload factors and overturn factors increase as the angle of attack of wind load increases. The derailment quotients, offload factors and overturn factors for a vehicle model is presented in terms of linear and nonlinear creep models. In general, when cross-wind loads are considered to act on the car body, the derailment quotients, offload factors and overturn factors that are determined by the nonlinear creep model are consistently higher than those evaluated from the linear creep model. As a result, the angle of attack of the wind load has a significant effect on the derailment safety assessment for a railway vehicle system.

INTRODUCTION

A railway vehicle system uses aerodynamic design, regenerative braking, engine technology and dynamic weight shifting. Railway vehicle systems are constructed to condense the travelling time between two cities. In past decades the elimination of the risk of derailment has become increasingly important.

For a traditional railway vehicle system, there are several nonlinear parameters, for example, suspension forces, wheel-rail normal forces, wheel taper profile and nonlinear contact forces and moments. The dynamic behavior of railway vehicles running on curved tracks are examined by some studies (Cheng and Hsu, 2012; Auciello et al., 2009; Cheng and Lee, 2011; Xiao et al., 2012). Running safety assessment is a significant aspect of the dynamic analysis of a railway vehicle. Several studies present mechanisms for derailment for a railway vehicle system running on a tangent or on curved tracks. The critical speeds for impact derailment evaluated by the nonlinear creep method are studied by Wang and Li (2010). Durali and Jalili (2010) determined the capability to forecast the derailment safety using a new derailment criterion. Considers the horizontal component of the tangential force at the contact point, Kuo and Lin (2015) developed a derailment criterion. He et al. (2015) used a survival model that assesses the derailment risk as a function of track defects and traffic conditions.

As well as the effect of track irregularities on derailment risk some literatures determine the effect of crosswind loads on the dynamic safety and risk of derailment for a railway vehicle system. Using a linear creep model, Xu et al. (2003) and Zhang et al. (2018) determined the dynamic response and risk of derailment for a bridge-train system. Cheng et al. (2011) and Zeng et al. (2016) presented the dynamic behavior and instability mode for a traditional railway vehicle system that is subjected to aerodynamic forces. For cross-winds at various angles of attack, Bocciolone et al. (2008), Han et al. (2014) and Baker et al. (2009) illustrated the dynamic response analysis for a traditional railway vehicle model.

Although the risk of derailment for a vehicle model subjected to rail irregularities and cross-wind loads was described by Cheng et al. (2013), the angle

Paper Received Apirl, 2019. Revised May, 2019, Accepted July, 2019, Author for Correspondence: Yung-Chang Cheng.

* *Professor, Department of Mechanical Engineering, National Kaohsiung University of Science and Technology, Kaohsiung, Taiwan 9182.*

** *Professor, Department of Civil and Environmental Engineering, National University of Kaohsiung, Kaohsiung, Taiwan 91811.*

*** *Assistant Professor, Department of Aircraft Engineering, Air Force Institute of Technology, Kaohsiung, Taiwan 91820.*

of attack for the cross-wind load is assumed to be constant. Using the linear creep forces and moments, the effect of the angle of attack of cross-wind aerodynamic forces on the dynamic response of a railway vehicle model was determined by Bocciolone et al. (2008), Han et al. (2014) and Baker et al. (2009). When cross-wind forces act on the car body, the overturn factor is a significant factor in the risk of derailment. However, the overturn factor is rarely used by these studies for derailment safety analysis. Therefore, the principal contribution of this paper is an analysis and comparison of the effects of cross-wind loads at different angles of attack on the derailment quotients, offload factors and overturn factors when rail irregularities are considered in the railway vehicle model with linear and nonlinear creep modes.

This paper determines the nonlinear differential equations of motion for a freight railway vehicle constructed by a 31-DOF system evaluated via the heuristic nonlinear creep model and subjected to rail irregularities and various cross-wind loads. In each wheelset model, it contains the lateral displacement, vertical displacement, roll angle and yaw angle. In the bogie frames and the car body models, it contains the lateral displacement, vertical displacement, roll angle, pitch angle and yaw angle. Employing the Runge-Kutta fourth-order method, the derailment quotients, offload factors and overturn factors are evaluated for different speeds and angles of attack for a wind load. The numerical results show how the vehicle speed affect the derailment quotients, offload factors and overturn factors under rail irregularities and varying angles of attack of wind loads. Finally, the effects of the vehicle speed on the derailment quotients, offload factors and overturn factors are illustrated and compared for wind loads at different angles of attack by linear and nonlinear creep models.

DIFFERENTIAL EQUATIONS OF MOTION

Rail Irregularities

Rail irregularities are an important issue for the derailment safety and ride comfort of a railway vehicle system. This study considers rail irregularities in the lateral and vertical directions. A study of high frequency irregularities in Germany railways (ORE, 1987) showed that the power spectrum densities for the rail irregularity in the lateral direction, $S_a(\Omega)$, and the vertical direction, $S_v(\Omega)$ are given by:

$$S_a(\Omega)=\frac{A_a\Omega_c^2}{\left(\Omega^2+\Omega_r^2\right)\left(\Omega^2+\Omega_c^2\right)}, \tag{1a}$$

$$S_v(\Omega)=\frac{A_v\Omega_c^2}{\left(\Omega^2+\Omega_r^2\right)\left(\Omega^2+\Omega_c^2\right)}, \tag{1b}$$

where Ω is the space frequency. A_a and A_v indicate the roughness constants in the lateral and vertical directions. Ω_c and Ω_r denote the cut-off frequencies. In addition, A_a, A_v, Ω_c and Ω_r are given in Appendix(II). The vehicle speed of 120 km/h is assumed to use for calculating the simulated rail irregularities data by MATLAB programs. Then, the rail irregularities in the space domain are calculated via the random number generator and the Inverse Fast Fourier Transform (IFFT) in MATLAB software. Therefore, the rail irregularities in the lateral (y_{rij}) and vertical (z_{rij}) directions are shown in Figure 1. Additionally, the external forces acting on the wheelsets due to rail irregularities are given as:

$$F_{ryij}=K_{ry}y_{rij}, \tag{2}$$

$$F_{rzij}=K_{rz}z_{rij}, \tag{3}$$

where K_{ry} and K_{rz} are the contact stiffness between wheels and rails in the lateral and vertical directions, respectively. (Sezer and Atalay, 2011)

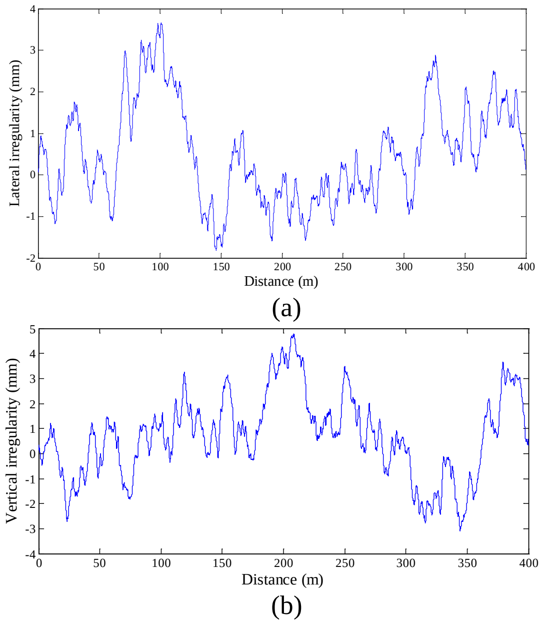

Fig. 1. Rail irregularities acting on the wheelsets in: (a) the lateral direction and (b) the vertical direction

Wind Loads

This study considers the cross-wind load that acts on the car body, including the static and buffeting loads (Figure 2). The wind load also acts on the car body at different angles of attack (Bocciolone *et al.*, 2008). In Figure 2(b), θ_{at} is the angle of attack of the wind loads that act on the car body. This is defined as the angle between the direction of the vehicle motion and the mean direction of the wind. The wind load is composed of a drag force, $F^D(t)$, a lift force, $F^L(t)$ and a pitch moment, $F^M(t)$, which are described as (Li et al., 2005, Cheng et al., 2013 and Bocciolone et al., 2008):

$$F^D(t)=\frac{1}{2}\rho\left(U+u(t)\right)^2 C_D(\theta_{at})HL\,, \tag{4}$$

$$F^L(t)=\frac{1}{2}\rho\left(U+w(t)\right)^2 C_L(\theta_{at})BL\,, \tag{5}$$

$$F^M(t)=\frac{1}{2}\rho\left[\left(U+u(t)\right)^2+\left(w(t)\right)^2\right]C_M(\theta_{at})B^2L\,, \tag{6}$$

where $C_D(\theta_{at})$, $C_L(\theta_{at})$, and $C_M(\theta_{at})$ are the drag, lift, and moment coefficients in terms of the angle of attack, as shown in Figure 3 (Bocciolone et al., 2008). ρ is regarded as the air density, and H means the height of the car body vertical to the main stream direction. B denotes as the width of the car body along the mean wind flow, and L denotes the length of the car body. U denotes the mean wind speed and $u(t)$ and $w(t)$ are defined as the along-wind and vertical components of the fluctuation on the wind velocity, respectively (Figure 4). These are described by their auto-spectral density functions developed by Simiu and Scanlan (1996) given as: (Yang et al., 2001):

$$\frac{\omega S_{uu}(\omega)}{u_*^2}=\frac{200f}{\left(1+50f\right)^{5/3}}\,, \tag{7}$$

$$\frac{\omega S_{ww}(\omega)}{u_*^2}=\frac{3.36f}{\left(1+10f^{5/3}\right)}\,, \tag{8}$$

where S_{uu} and S_{ww} denote the auto-spectral density functions for $u(t)$ and $w(t)$. Therefore, $u(t)$ and $w(t)$ can be found from the Inverse Fast Fourier Transformation for S_{uu} and S_{ww} (Cheng et al., 2013).

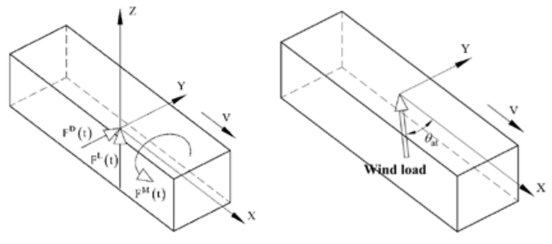

(a) (b)

Fig. 2. Wind load acting on the car body

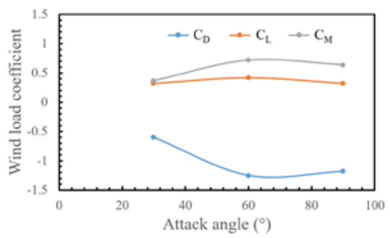

Fig. 3. The coefficients of drag, lift and moment in terms of the angle of attack

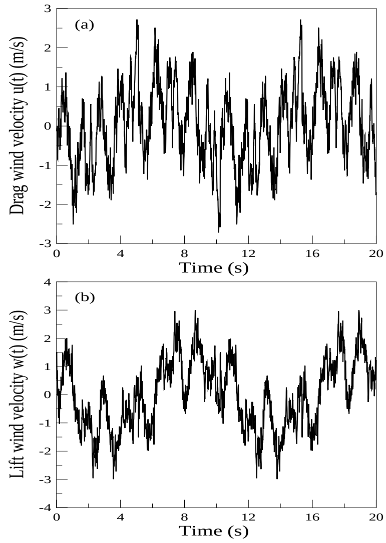

Fig. 4. The time histories for the fluctuations in wind velocity at an average wind speed $U=17.2$ m/s for: (a) along-wind u(t) and (b) vertical component w(t)

Nonlinear Creep Model

This study determines the nonlinear differential equations of motion for a 31-DOF railway vehicle model. The main nonlinear terms are the nonlinear creep forces and moments. The contact forces between the rails and the wheels are created using a heuristic nonlinear creep model which calculated from Kalker's linear creep theory (Dukkipati and Garg, 1984) with creep force saturation. The saturation constant, α_{ij}, and the nonlinear creep forces, $F^n_{kxij}(y_{wij},\dot{y}_{wij},\psi_{wij},\dot{\psi}_{wij})$ and $F^n_{kyij}(y_{wij},\dot{y}_{wij},\psi_{wij},\dot{\psi}_{wij})$, and the nonlinear creep moment, $M^n_{kzij}(y_{wij},\dot{y}_{wij},\psi_{wij},\dot{\psi}_{wij})$, are used, as given by (Cheng and Hsu, 2016):

$$F^n_{kxij}(y_{wij},\dot{y}_{wij},\psi_{wij},\dot{\psi}_{wij})=\alpha_{ij}F_{kxij}\,, \tag{9}$$

$$F^n_{kyij}(y_{wij},\dot{y}_{wij},\psi_{wij},\dot{\psi}_{wij})=\alpha_{ij}F_{kyij}\,, \tag{10}$$

$$M^n_{kzij}(y_{wij},\dot{y}_{wij},\psi_{wij},\dot{\psi}_{wij})=\alpha_{ij}M_{kzij}\,, \tag{11}$$

where subscripts $k=L,\,R$ respectively specify the left and right wheels, the subscripts $i=1,\,2$ respectively specify the front and rear of the bogie frame and the subscripts $j=1,\,2$ respectively specify the front and rear wheel-sets. F_{kxij}, F_{kyij} and M_{kzij} are the linear creep forces and the creep moments that are calculated using Kalker's linear theory after the coordinate transformation and are given by (Cheng and Hsu, 2016)

$$F_{Lxij}=F^*_{Lxij}-F^*_{Lyij}\psi_{wij}\,, \tag{12a}$$

$$F_{Lyij}=F^*_{Lxij}\psi_{wij}+F^*_{Lyij}\,,\quad M_{Lzij}=M^*_{Lzij} \tag{12b}$$

$$F_{Rxij}=F^*_{Rxij}-F^*_{Ryij}\psi_{wij}\,, \tag{13a}$$

$$F_{Ryij} = F^{*}_{Rxij}\psi_{wij} + F^{*}_{Ryij}\,,\quad M_{Rzij} = M^{*}_{Rzij} \tag{13b}$$

where, F^{*}_{kxij}, F^{*}_{kyij} and M^{*}_{kzij} denote the creep forces and moments that are evaluated from Kalker's linear theory (Dukkipati and Garg, 1984) directly on the contact points and are shown in Cheng and Hsu (2016). The saturation constant α_{ij} in Equations (9) ~ (11) is calculated as:

$$\alpha_{ij} = \begin{cases} \dfrac{1}{\beta_{ij}}\left[\beta_{ij} - \dfrac{1}{3}\beta_{ij}^{\;2} + \dfrac{1}{27}\beta_{ij}^{\;3}\right] & \text{for} \quad \beta_{ij} \le 3 \\ \dfrac{1}{\beta_{ij}} & \text{for} \quad \beta_{ij} \ge 3 \end{cases}, \tag{14}$$

where β_{ij} is the nonlinearity that is obtained from the resultant forces, which are evaluated from the linear creep forces and moments. As the saturation constant $\alpha_{ij} = 1$ or $\alpha_{ij} = \text{constant}$, the nonlinear creep model can be reduced to the Kalker's linear model. The relation between the nonlinear creep model and Kalker's linear model is represented by Figure 5. When the creepage ξ of the creep force is getting larger, the non-dimensional traction F/fN equals to 1 for the nonlinear creep model. The non-dimensional traction F/fN denotes the nonlinearity β_{ij}. As F/fN equals to 1, the nonlinear creep model is closed to Kalker's linear model.

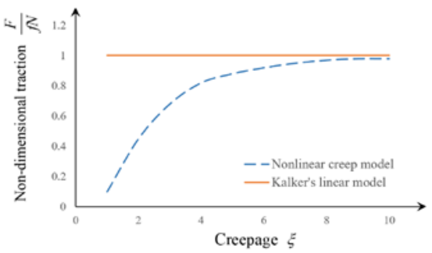

Fig. 5. Comparsion of the nonlinear creep model and Kalker's linear model.

Motion of the Bogie Frame and the Car Body

This study determines the derailment risk for a 31-DOF railway vehicle model that moves on the circular curved tracks with the constant radius, R (Figure 6). The 31 DOFs of the vehicle model is given in Appendix (I). The simple sketch of the vehicle model is given as shown in Figure 7. The equations of motion for the bogie frame are: (Dukkipati and Garg, 1984)

lateral displacement (y_{ti}) :

$$m_t \ddot{y}_{ti} = F_{syti} + (\frac{V^2}{gR} - \phi_{se}) m_t g\,, \tag{15}$$

vertical displacement (z_{ti}):

$$m_t \ddot{z}_{ti} = F_{szti} - \left(1 + \frac{V^2}{gR}\phi_{se}\right) m_t g\,, \tag{16}$$

roll angle (ϕ_{ti}): $I_{tx}\ddot{\phi}_{ti} = M_{sxti}\,,$ (17)

pitch angle (θ_{ti}): $I_{ty}\ddot{\theta}_{ti} = M_{syti}\,,$ (18)

yaw angle (ψ_{ti}): $I_{tz}\ddot{\psi}_{ti} = M_{szti}\,,$ (19)

The equations of motion for the car body are:

lateral displacement (y_c):

$$m_c \ddot{y}_c = F_{syc} + (\frac{V^2}{gR} - \phi_{se}) m_c g + F^D(t)\,, \tag{20}$$

vertical displacement (z_c):

$$m_c \ddot{z}_c = F_{szc} - \left(1 + \frac{V^2}{gR}\phi_{se}\right) m_c g + F^L(t)\,, \tag{21}$$

roll angle (ϕ_c): $I_{cx}\ddot{\phi}_c = M_{sxc} + F^M(t)\,,$ (22)

pitch angle (θ_c): $I_{cy}\ddot{\theta}_c = M_{syc}\,,$ (23)

yaw angle (ψ_c): $I_{cz}\ddot{\psi}_c = M_{szc}\,,$ (24)

where V is the velocity of the railway vehicle and ϕ_{se} means the super-elevation angle of the circular curved tracks. Additionally, the suspension forces and the moments on the car body and each bogie frame, F_{syc}, F_{syti}, F_{szc}, F_{szti}, M_{sxc}, M_{sxti}, M_{syc}, M_{syti}, M_{szc} and M_{szti}, are given in Cheng and Hsu (2016).

Fig. 6. Car body model

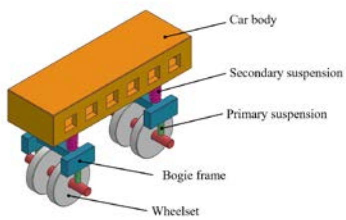

Fig. 7. 3D vehicle model

Motion of Wheelsets

Using the nonlinear creep model to model the relationship between wheels and rails and considering the rail irregularities for curved tracks, the combined equations of motion for each wheelset are described as (Figure 8):

lateral displacement (y_{wij}):

$$\begin{aligned} m_w\left(\ddot{y}_{wij}-\frac{V^2}{R}\right) &= -\frac{2\alpha_{ij} f_{11}}{V}\left(\dot{y}_{wij}-V\psi_{wij}\right) \\ &-\frac{2\alpha_{ij} f_{12}}{V}\left(\dot{\psi}_{wij}-\frac{V}{R}\right)-\frac{2r_0\alpha_{ij} f_{11}}{V}\dot{\phi}_{wij} \\ &-\left[\left(W_{ext}+m_w g\right)+\frac{V^2W_{ext}}{gR}\phi_{se}\right]\phi_{wij} \\ &-\left(W_{ext}+m_w g\right)\phi_{se}+\frac{V^2W_{ext}}{gR}+F_{syij}+F_{ryij} \end{aligned} , \quad (25)$$

vertical displacement (z_{wij}):

$$\begin{aligned} m_w\left(\ddot{z}_{wij}+\frac{V^2}{R}\phi_{se}\right) &= -\frac{2\lambda^2\alpha_{ij} f_{11}}{V}y_{wij}\dot{\phi}_{wij} \\ &-\frac{2\alpha_{ij} f_{11}}{V}\dot{y}_{wij}\phi_{wij}-\frac{2\alpha_{ij} f_{12}}{V}\phi_{wij}\dot{\psi}_{wij}+F_{szij}+F_{rzij} \\ &-\frac{2r_0\alpha_{ij} f_{11}}{V}\phi_{wij}\dot{\phi}_{wij}+\frac{2\lambda^2\alpha_{ij} f_{12}}{r_0}+\frac{2\alpha_{ij} f_{12}}{R}\phi_{wij} \end{aligned} , \quad (26)$$

roll angle (ϕ_{wij}):

$$\begin{aligned} I_{wx}\ddot{\phi}_{wij}-I_{wy}\left(\frac{V}{r_0}\right)\left(\dot{\psi}_{wij}-\frac{V}{R}\right) &= \frac{2\lambda^2\alpha_{ij} f_{12}}{r_0}y_{wij} \\ &-\left(W_{ext}+m_w g+\frac{V^2W_{ext}}{gR}\phi_{se}\right)\lambda^2 y_{wij}+2\lambda^2\alpha_{ij} f_{12}\phi_{wij} \\ &-\frac{2\alpha_{ij} f_{11}(a\lambda+r_0)}{V}\dot{y}_{wij}-\frac{2r_0\alpha_{ij} f_{11}}{V}\left(a\lambda+r_0\right)\dot{\phi}_{wij} \\ &+\left(W_{ext}+m_w g+\frac{V^2W_{ext}}{gR}\phi_{se}\right)a\lambda\phi_{wij}+M_{sxij} \\ &-\frac{2\alpha_{ij} f_{12}}{V}\left(a\lambda+r_0\right)\dot{\psi}_{wij}+\frac{2\alpha_{ij} f_{12}}{R}\left(a\lambda+r_0\right) \\ &+\left[2\alpha_{ij} f_{11}(a\lambda+r_0)+\frac{2\alpha_{ij}\lambda^2 f_{22}}{r_0}\right]\psi_{wij}+M_{exij} \end{aligned} , \quad (27)$$

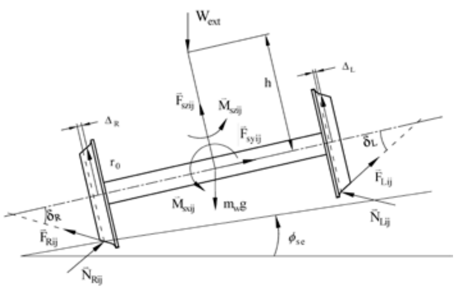

Fig. 8. Free body diagram of a single wheelset

yaw angle (ψ_{wij}):

$$\begin{aligned} I_{wz}\ddot{\psi}_{wij} &= -\frac{2a\lambda\alpha_{ij} f_{33}}{r_0}y_{wij}+\frac{2\alpha_{ij} f_{12}}{V}\dot{y}_{wij} \\ &-\left(I_{wy}\frac{V}{r_0}-\frac{2r_0\alpha_{ij} f_{12}}{V}\right)\dot{\phi}_{wij}-2\alpha_{ij} f_{12}\psi_{wij} \\ &+\left(W_{ext}+m_w g+\frac{V^2W_{ext}}{gR}\phi_{se}\right)a\lambda\psi_{wij}+M_{szij} \\ &-\left(\frac{2a^2\alpha_{ij} f_{33}}{V}+\frac{2\alpha_{ij} f_{22}}{V}\right)\dot{\psi}_{wij}+\frac{2\alpha_{ij}}{R}\left(a^2 f_{33}+f_{22}\right) \end{aligned} , \quad (28)$$

where $\alpha_{ij}=\alpha_{ij}\left(y_{wij},\dot{y}_{wij},\psi_{wij},\dot{\psi}_{wij}\right)$. The suspension forces and the moments on each wheelset, F_{syij}, F_{szij}, M_{exij}, M_{sxij} and M_{szij}, are respectively expressed in Cheng and Hsu (2106). As a result, the nonlinear governing equations of motion of a 31-DOF railway vehicle model are created and composited using Equations (15)–(28).

DERAILMENT SAFETY ANALYSIS

Risk of derailment is the most important dynamic behavior for railway vehicles. Consequently, in this paper, the derailment quotient and the offload factor determine the running safety for a railway vehicle that moves on curved tracks. Derailment quotient is the ratio of lateral to vertical forces on a climbing wheel. It means the limit of the ratio as the wheel climbs on or climb out the rail. If the real dynamic ratio of lateral to vertical forces is lower than the specified derailment quotient, the railway vehicle system is safe. According to Cheng and Hsu (2012), the derailment quotient for a wheelset is given as (Figure 9):

$$\frac{Q_{kij}}{P_{kij}}=\frac{F_{kyij}^{n}+N_{kyij}}{F_{kzij}^{n}+N_{kzij}}, \quad (29)$$

where Q_{kij} and P_{kij} are the contact forces due to a single side wheel acting in the lateral and vertical directions, respectively, F_{kyij}^{n} and F_{kzij}^{n} denote the creep forces that act in the lateral and vertical directions, respectively. N_{kyij} and N_{kzij} denote the normal forces that act in the lateral and vertical direction, respectively, as shown in Cheng and Hsu (2012). Using the Runge-Kutta fourth-order method, the all displacements and velocities can be found. Then, the creep forces that act in the lateral and vertical directions, and the normal forces that act in the lateral and vertical direction are calculated. Therefore, the dynamic derailment quotient is obtained by Equation (29).

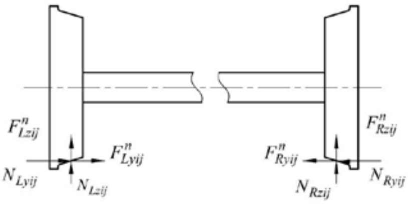

Fig. 9. Contact forces on the left and right wheels

The offload factor is another index for the risk of derailment. This is expressed by the ratio of the reduction in the vertical force to the static wheel load in the vertical direction. In the curving negotiation, when the differences in wheel loads of the right and left side wheel are too large, the reduction in the vertical force is increased. Therefore, if the real dynamic ratio of the reduction in the vertical force to the static wheel load is larger than the specified offload factor, the railway vehicle system is dangerous with derailment risk. Because of including the nonlinear creep forces and the normal forces in the vertical direction, the offload factor for a wheel can be accurately calculated as (Cheng and Hsu, 2016 and Xia et al., 2000):

$$\frac{\Delta P_{kij}}{P_{S,kij}} = \frac{P_{Sij} - P_{kij}}{P_{S,kij}}, \tag{30}$$

where ΔP_{kij} is the reduction in the vertical force and $P_{S,kij}$ is the static wheel load for a single side wheel. Using the Runge-Kutta fourth-order method, the all displacements and velocities can be found. The vertical force acting on the right and left side wheels is calculated from Equation (26). Therefore, the reduction force between the right and left side wheels can be found. The static wheel load for a single side wheel is determined by the wheel external loads and axle loads W_{ext}. As a result, the dynamic offload factor is obtained by Equation (30).

The overturn factor is also an index for the risk of derailment. The overturn factor determines whether the train will overturn when it is subjected to external forces such as wind load, centrifugal force and lateral vibrational inertial force. The overturn factor is the ratio of the lateral load acting on vehicle to the static wheel load. The lateral loads acting on vehicle includes the wind loads and centrifugal forces. However, if the dynamic lateral load is getting larger, the real dynamic ratio of the lateral load acting on vehicle to the static wheel load is higher than the specified offload factor. Therefore, the railway vehicle system is dangerous with derailment risk. The overturn factor for a wheelset is calculated using the equation that was derived by (Lei, 2017 and Andersson et al., 2004):

$$D = \frac{P_d}{P_{st}}, \tag{31}$$

where P_d is the dynamic lateral load on the vehicle and P_{st} is the static wheel load. Using the Runge-Kutta fourth-order method, the all displacements and velocities can be found. The dynamic lateral force acting on the vehicle including wind loads, centrifugal forces and lateral vibrational inertial forces are calculated from Equations (15), (20) and (25). The static wheel load for a single side wheel is determined by the wheel external loads and axle loads W_{ext}. As a result, the dynamic overturn factor is obtained by Equation (31).

Three derailment assessment coefficients have been presented in Equations (29)-(31). In order to ensure the running safety, the derailment criterion for three coefficients has to be specified. According to the safety criteria in Japan railway system and Xiao et al. (2012), the derailment safety assessment criteria is given as:

(1) Derailment quotient: $\frac{Q_{kij}}{P_{kij}} < 0.8$, (32a)

(2) Offload factor: $\frac{\Delta P_{kij}}{P_{S,kij}} < 0.8$, (32b)

(3) Overturn factor: $D = \frac{P_d}{P_{st}} < 0.8$, (32c)

NUMERICAL RESULTS

In this study, the system parameters that are given in Appendix (II), which are from the studies by Cheng et al. (2013), Sezer and Atalay (2011), Bocciolone et al. (2008) and Ahmed and Sankar (1987), are used to study the derailment quotient, offload factor and overturn factor of different physical parameters. The system parameters value is the freight railway vehicle system. In order to simulate the different angle of attack how to affect the derailment safety, the car body parameters is referred to Bocciolone et al. (2008). Using the Runge-Kutta fourth-order method, the lateral displacement, the vertical displacement, the roll angle and the yaw angle for each wheelset are calculated. In this paper, it assumes that the trade profile of the wheel that is used to calculate the risk of derailment indices is also perfectly conical. Additionally, the length of the time step for the dynamic analysis program is the same as the time history for the cross-wind loads.

In the numerical analysis, all of the initial conditions are set to be zero simplicity. According to Equations (29)-(31), the derailment quotients, offload factors and overturn factors are calculated from dynamic response of the 31-DOF vehicle model. In Figures 10-12, the effects of the vehicle speed on the derailment quotients, offload factors and overturn factors for the 31-DOF vehicle model subjected to rail irregularities and wind load at different angles of attack are shown.

Figure 10 shows how the vehicle speed affects the derailment quotients and offload factors under the wind loads at different angles of attack. Figure 10(a) shows that for the railway vehicle model that is not subject to wind load, the derailment quotient increases slowly when the vehicle speed is increased. When the wind load is applied to act on the car body, the derailment quotient increases when the vehicle speed is increased. Moreover, the derailment quotient also increases when the angle of attack of the wind load increases. Figure 10(b) shows that for a railway vehicle model that is not subject to a wind load, the vehicle speed has a negligible effect on the offload factor. However, the offload factor increases while the vehicle speed is increased when the wind load is taken into account. The offload factor also increases as the angle of attack of the wind load is increased so the danger is more significant when the angle of attack of the wind load increases. According to the derailment criterion described in Equation (32), the safety region for derailment quotient is presented in Figure 10(a), and the safety region for offload factor is shown in Figure 10(b). If the derailment quotient and offload factor are lower than 0.8, the railway vehicle is safe for the derailment quotient and offload factor. From these two Figures, the railway vehicle without wind loads and rail irregularities is safe for the derailment quotient and offload factor.

Figure 11 compares how the vehicle speed affects the derailment quotients and offload factors for a vehicle model subjected to rail irregularities and cross-wind loads at different angles of attack. When rail irregularities and cross-wind loads are applied to the railway vehicle model, the derailment quotient and the offload factor increase when the vehicle speed is increased. The derailment quotient and the offload factor increase when the angle of attack of the wind load increases. Figure 11(a) shows that for a railway vehicle model subjected to rail irregularities and no wind load, the derailment quotient increases smoothly when the vehicle speed is increased. A comparison of Figures 8 and 9 shows that the derailment quotient and the offload factor increase if the rail irregularities and the wind load are considered to act simultaneously on the railway vehicle system. According to the derailment criterion described in Equation (32), the safety region for derailment quotient is presented in Figure 11(a), and the safety region for offload factor is shown in Figure 11(b). From these two Figures, the railway vehicle under rail irregularities and without wind loads is safe for the derailment quotient and offload factor. Moreover, when the rail irregularities and wind loads with 90° angles of attack act on the railway vehicle, the railway vehicle model is dangerous for the derailment quotient and offload factor in all vehicle speeds.

Figure 12 presents how the vehicle speed affects the overturn factors for the railway vehicle model subjected to rail irregularities and cross-wind loads at different angles of attack. Figure 12(a) shows that for the vehicle model that is not subject to rail irregularities or wind load, the overturn factor decreases and then increases while the vehicle speed is increased. However, when the wind load is considered to act on car body, the overturn factor increases while the vehicle speed is increased. Figure 12(b) shows that the difference in the value for the overturn factor for different angles of attack can be neglected when the vehicle speed is generally less than 200 km/h. However, the angle of attack of the wind load has a significant effect on the overturn factor when the vehicle speed is consistently higher than 200 km/h. According to the derailment criterion described in Equation (32), the safety region for overturn factor is presented in Figures 12(a) and 12(b). From these two Figures, the railway vehicle under rail irregularities and without wind loads is safe for the overturn factor. In Figure 12(a), when the rail irregularities are not considered and the angle of attack is 30°, the railway vehicle model is safe for the overturn factor. However, in Figure 12(b), when the rail irregularities and wind loads with 60° and 90° angles of attack, the railway vehicle model is dangerous for the overturn factor in all vehicle speeds.

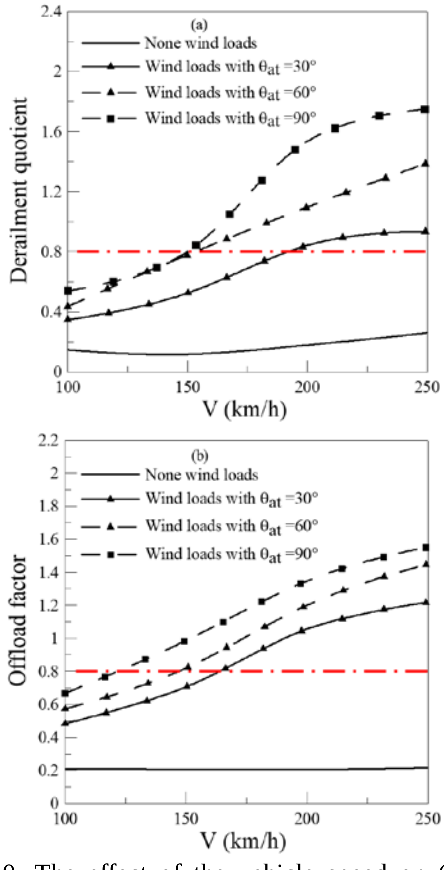

Fig. 10. The effect of the vehicle speed on (a) the derailment quotient and (b) the offload factor for wind loads at different angles of attack.

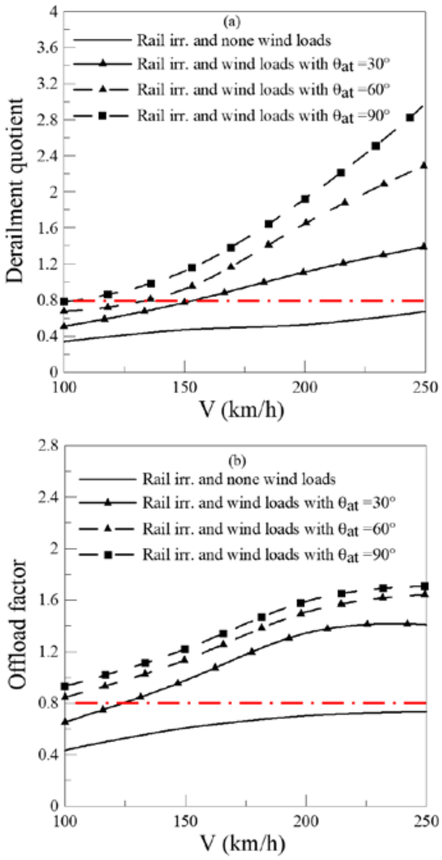

Fig. 11. The effect of the vehicle speed on (a) the derailment quotient and (b) the offload factor when the system is subjected to rail irregularities and wind loads at different angles of attack

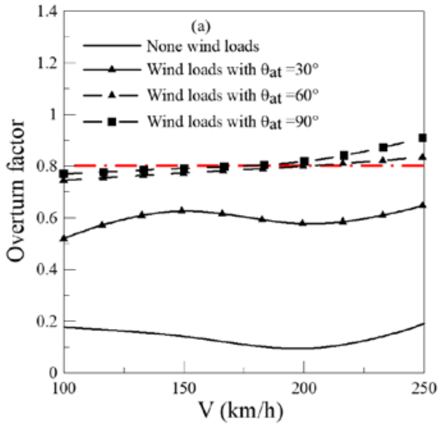

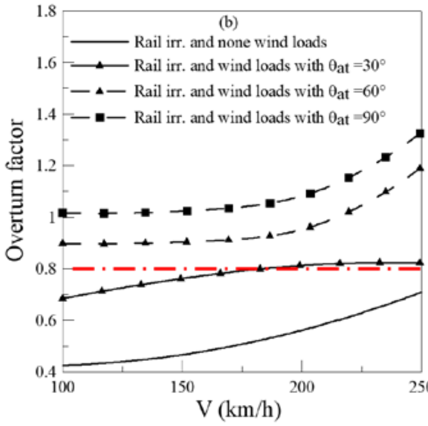

Fig. 12. The effect of the vehicle speed on the overturn factor for (a) wind loads at different angles of attack and (b) rail irregularities and wind loads at different angles of attack

Effects of the Vehicle Speed on Derailment Quotients, Offload Factors and Overturn Factors for Linear and Nonlinear Creep Models

Figure 13 reveals how the vehicle speed affects the derailment quotient evaluated via linear and nonlinear creep models and cross-wind load at different angles of attack. The numerical results in Figure 13 show that the derailment quotient evaluated via the nonlinear creep model is generally larger than that obtained from the linear creep model. For the linear creep model, the derailment quotient increases when the vehicle speed is increased. Furthermore, the derailment quotient also increases when the angle of attack of the wind load is increased. According to the derailment criterion described in Equation (32), the safety region for derailment quotient is determined. In Figure 13, the railway vehicle model is safe for the derailment quotient evaluated by the linear creep model as the angles of attack are 30° and 60°. It shows that the running safety of a railway vehicle model is overestimated as the linear creep model is applied to simulate the contact forces between wheels and rails.

Figure 14 shows the effect of the vehicle speed on the offload factor for a railway vehicle model that uses the linear and nonlinear creep models with wind loads at different angles of attack. The offload factor evaluated via the nonlinear creep model is significantly greater than that obtained from the linear creep model. Additionally, the offload factor evaluated via the linear creep model also increases when the vehicle speed and the angle of attack of the wind load are increased. According to the derailment criterion described in Equation (32), the safety region for the offload factor is given. In Figure 14, the railway vehicle model is generally safe for the offload factor evaluated by the linear creep model. As the vehicle speed is higher than 210 km/h, the railway vehicle is dangerous for the offload factor under 60° angle of attack. Therefore, in the most of cases, the running safety of a railway vehicle system considered the linear creep model is overestimated.

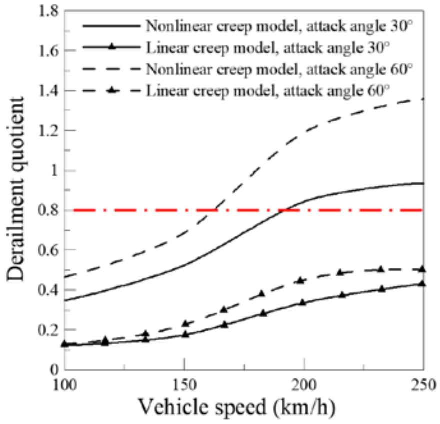

Fig. 13. The effect of the vehicle speed on the derailment quotient for linear and nonlinear creep models for angles of attack of $\theta_{st} = 30°$ and $\theta_{st} = 60°$ under no rail irregularities

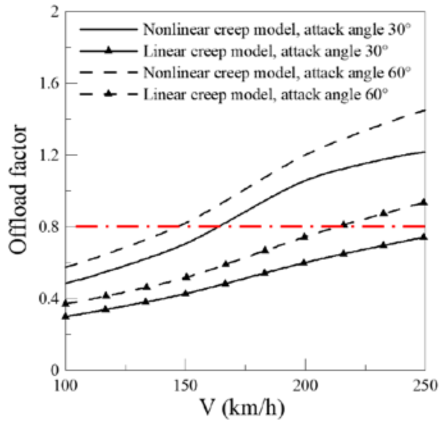

Fig. 14. The effect of the vehicle speed on the offload factor for linear and nonlinear creep models for angles of attack of $\theta_{st} = 30°$ and $\theta_{st} = 60°$ under no rail irregularities

CONCLUSIONS

Nonlinear differential equations of motion of the freight wagon railway vehicle system constructed by a 31-DOF model traveling on curved tracks are derived by a heuristic nonlinear creep model under rail irregularities and cross-wind loads. The derailment quotients, offload factors and overturn factors are examined by the derailment criterion. The effects of the vehicle speed on derailment quotients, offload factors and overturn factors under rail irregularities and wind loads at different angles of attack are determined. Previous studies do not consider this scenario. The derailment quotients, offload factors and overturn factors all increase when the vehicle speed and the angle of attack of the wind load are increased. Therefore, the risk of derailment for a railway vehicle system is significantly affected by rail irregularities and wind loads at different angles of attack.

Considering the linear and nonlinear creep models, the effects of the vehicle speed on derailment quotients, offload factors and overturn factors when the system is subject to wind loads at different angles of attack is also determined and compared. For these two creep models, the derailment quotient, the offload factor and the overturn factor generally increase when the vehicle speed is increased. The derailment quotients, offload factors and overturn factor for the nonlinear creep model are significantly higher than those for the linear creep model. However, when the vehicle speed consistently exceeds 180 km/h, the overturn factors for the linear creep model is greater than that for the nonlinear creep model. Finally, according to the derailment criterion description, the safety regions are presented for the derailment quotient, offload factor and overturn factor. In general, the running safety of a railway vehicle model is overestimated as the linear creep model is applied to simulate the contact forces between wheels and rails.

ACKNOWLEDGEMENT

The authors gratefully acknowledge the financial support of the Ministry of Science and Technology of Taiwan under Grant no. MOST 107-2221-E-992-038-MY2.

REFERENCES

Ahmadian M. and Yang S., “Effect of System Nonlinearities on Locomotive Bogie Hunting Stability,” *Vehicle System Dynamics*, Vol. 29, No. 6, pp. 366–384 (1998).

Ahmed, A. K. W. and Sankar S., “Lateral Stability Behavior of Railway Freight Car System with Elasto-Damper Coupled Wheelset: Part 2 - Truck Model,” *Transactions of the ASME, Journal of Mechanisms, Transmissions, and Automation in Design*, Vol. 109, No. 4, pp. 500-507 (1987).

Andersson, E., Haggstrom, J., Sima, M. and Satichel, S., “Assessment of Train-Overturning Risk Due to Strong Cross-Winds,” *Proceedings of the Institution of Mechanical Engineers, Part F: Journal of Rail and Rapid Transit*, Vol. 218, No. F3, pp. 213–223 (2004).

Auciello, J., Meli, E., Falomi, S. and Malvezzi, M., “Dynamic simulation of railway vehicles: wheel/rail contact analysis,” *Vehicle System Dynamics*, Vol. 47, No. 7, pp. 867–899 (2009).

Baker, C., Cheli, F., Orellano, A., Paradot, N., Proppe, C. and Rocchi, D., “Cross-wind Effects on Road and Rail Vehicles," *Vehicle System Dynamics*, Vol. 47, No. 8, pp. 983–1022 (2009).

Bocciolone, M., Cheli, F., Corradi, R., Muggiasca, S. and Tomasini, G., "Crosswind Action on Rail Vehicles: Wind Tunnel Experimental Analyses," *Journal of Wind Engineering and Industrial Aerodynamics*, Vol. 96, No. 5, pp. 584–610 (2008).

Cheng, Y. C. and Lee, C. H., "Hunting Stability Analysis of Titling Railway Vehicle with Actuator Controller," *Journal of the Chinese Society of Mechanical Engineers*, Vol. 32, No. 2, pp.119-130 (2011).

Cheng, Y. C., Chen, C. H. and Yang, C. J., "Dynamics Analysis of High-Speed Railway Vehicles Excited by Wind Loads," *International Journal of Structural Stability and Dynamics*, Vol. 11, No. 6, pp. 1103-1118 (2011).

Cheng, Y. C. and Hsu, C. T., "Hunting Stability and Derailment Analysis of A Car Model of High-Speed Railway System," *Proceedings of the Institution of Mechanical Engineers, Part F: Journal of Rail and Rapid Transit*, Vol. 226, No. 2, pp. 187–202 (2012).

Cheng, Y. C., Huang, C. H., Kuo C. M. and Chen, C. H., "Derailment Risk Analysis of A Tilting Railway Vehicle Moving over Irregular Tracks under Wind Loads," *International Journal of Structural Stability and Dynamics*, Vol. 13, No. 8, pp. 1350038-1~1350038-28 (2013).

Cheng, Y. C. and Hsu, C. T., "Parametric Analysis of Ride Comfort for Tilting Railway Vehicles Running on Irregular Curved Tracks," *International Journal of Structural Stability and Dynamics*, Vol. 16, No. 8, pp. 1550056-1 ~ 1550056-22 (2016).

Dukkipati, R. V., and Garg, V. K., Dynamics of Railway Vehicle Systems, Academic Press, Canada (1984).

Durali, M. and Jalili, M. M., "A New Criterion for Assessment of Train Derailment Risk," *Proceedings of the Institution of Mechanical Engineers, Part K: Journal of Multi-body Dynamics*, Vol. 224, No. 1, pp. 83–101 (2010).

Han, Y., Caia, C. S., Zhang, J., Chen, S. and He, X., "Effects of Aerodynamic Parameters on the Dynamic Responses of Road Vehicles and Bridges under Cross Winds," *Journal of Wind Engineering and Industrial Aerodynamics*, Vol. 134, pp. 78-95 (2014).

He, Q., Li, H., Bhattacharjya, D., Parikh, D. P. and Hampapur, A., "Track Geometry Defect Rectification Based on Track Deterioration Modelling and Derailment Risk Assessment," *Journal of the Operational Research Society*, Vol. 66, No. 3, pp. 392-404 (2015).

Kuo, C. M. and Lin, C. C., "Analysis of Derailment Criteria," *Proceedings of the Institution of Mechanical Engineers, Part F, Journal of Rail and Rapid Transit*, Vol. 230, No. 4, pp. 1158–1163 (2015).

Lei, X., High Speed Railway Track Dynamics: Models, Algorithms and Applications, Science Press, Beijing (2017).

Li Y. L., Qiang S. H., Liao H. L. and Xu Y. L., "Dynamics of Wind-Rail Vehicle-Bridge Systems," *Journal of Wind Engineering and Industrial Aerodynamics*, Vol. 93, pp. 483-507 (2005).

Office for Research and Experiments of the International Union of Railways (ORE), D161. Dynamic Vehicle/Track Interaction Phenomena, from the Point of View of Track Maintenance, in Report No.1: General conditions for the Study of the Evolution of Track Geometry Based on Historical Information, (Utrecht, 1987).

Sezer S. and Atalay A. E., "Dynamic Modeling and Fuzzy Logic Control of Vibrations of a Railway Vehicle for Different Track Irregularities," *Simulation Modelling Practice and Theory*, Vol. 19, No. 9, pp. 1873-1894 (2011).

Simiu E., and Scanlan R. H., Wind Effects on Structures: Fundamentals and Applications to Design, 3rd Edition, Wiley, New York (1996).

Wang, W. and Li G. X., "Development of a Simulation Model of a High-Speed Vehicle for a Derailment Mechanism," *Proceedings of the Institution of Mechanical Engineers, Part F: Journal of Rail and Rapid Transit*, Vol. 224, No. 2, pp. 103–113 (2010).

Xia, H., Xu, Y. L. and Chan, T. H. T., "Dynamic Interaction of Long Suspension Bridges with Running Trains," *Journal of Sound and Vibration*, Vol. 237, No. 2, pp. 263–280 (2000).

Xiao, X., Ling, L. and Jin, X., "A Study of the Derailment Mechanism of a High Speed Train due to an Earthquake," *Vehicle System Dynamics*, Vol. 50, No. 3, pp. 121–147 (2012).

Xu Y. L., Xia H. and Yan, Q. S., "Dynamic Response of Suspension Bridge to High Winds and Running Train," *Journal of Bridge Engineering*, Vol. 8, No. 1, pp. 46-55 (2003).

Yang Y. B., Mac S. V. and Chen C. H., "Multi-Mode Coupled Buffeting Analysis of Cable-Stayed Bridges," *International Journal of Structural Stability and Dynamics*, 1(3) (2001) 429-453.

Zeng, X., Wu, H., Lai, J. and Sheng, H., "Hunting Stability of High-Speed Railway Vehicles on A Curved Track Considering the Effects of Steady Aerodynamic Loads," *Journal of Vibration and Control*, Vol. 22, No. 20, pp. 4159-4175 (2016).

Zhang, X., Wen, Z., Chen, W., Wang, X. and Zhu, Y., "Dynamic Analysis of Coupled Train–Track–Bridge System Subjected to Debris Flow Impact," *Advances in Structural Engineering*, Vol. 22, No. 4, pp. 919-934 (2018).

APPENDIX(I): 31 DOFs vehicle model

Body		Degree of freedom
Front bogie	Front wheelset	Lateral displacement, vertical displacement, roll angle, yaw angle
	Rear wheelset	Lateral displacement, vertical displacement, roll angle, yaw angle
	Bogie frame	Lateral displacement, vertical displacement, roll angle, pitch angle, yaw angle
Rear bogie	Front wheelset	Lateral displacement, vertical displacement, roll angle, yaw angle
	Rear wheelset	Lateral displacement, vertical displacement, roll angle, yaw angle
	Bogie frame	Lateral displacement, vertical displacement, roll angle, pitch angle, yaw angle
Car	Car body	Lateral displacement, vertical displacement, roll angle, pitch angle, yaw angle

Appendix(II): System Parameters

Wheelsets:

Parameters	Value
Wheelset mass	$m_w = 1117.9$ kg
Roll moment of inertia of wheelset	$I_{wx} = 608.1$ kg-m^2
Spin moment of inertia of wheelset	$I_{wy} = 72$ kg-m^2
Yaw moment of inertia of wheelset	$I_{wz} = 608.1$ kg-m^2
Wheel radius	$r_0 = 0.43$ m
Half of track gauge	$a = 0.7175$ m
Wheel conicity	$\lambda = 0.05$
Lateral creep force coefficient	$f_{11} = 2.212\times10^6$ N
Lateral/spin creep force coefficient	$f_{12} = 3120$ N-m^2
Spin creep force coefficient	$f_{22} = 16$ N
Longitudinal creep force coefficient	$f_{33} = 2.563\times10^6$ N
Radius of curved tracks	$R = 6250$ m
Superelevation angle of curved track	$\phi_{se} = 0.0873$ rad
Axle load	$W_{ext} = 5.6\times10^4$ N
Contact stiffness in lateral direction between wheels and rails	$K_{ry} = 8.6\times10^7$ N/m
Contact stiffness in vertical direction between wheels and rails	$K_{rz} = 3.5\times10^{10}$ N/m

Bogie frame:

Parameters	Value
Bogie frame mass	$m_t = 350.26$ kg
Roll moment of inertia of bogie frame	$I_{tx} = 300$ kg-m^2
Yaw moment of inertia of bogie frame	$I_{tz} = 105.2$ kg-m^2

Car body:

Parameters	Value
Car body mass	$m_c = 8041.3$ kg
Roll moment of inertia of car body	$I_{cx} = 14270$ kg-m^2
Yaw moment of inertia of car body	$I_{cz} = 123760.5$ kg-m^2

Suspension systems:

Parameters	Value
Longitudinal stiffness of primary suspension	$K_{px} = 9\times10^5$ N/m
Lateral stiffness of primary suspension	$K_{py} = 3.9\times10^5$ N/m
Vertical stiffness of primary suspension	$K_{pz} = 6\times10^5$ N/m
Vertical damping of primary suspension	$C_{pz} = 4\times10^4$ N-s/m
Longitudinal stiffness of secondary suspension	$K_{sx} = 3.5\times10^4$ N/m
Lateral stiffness of secondary suspension	$K_{sy} = 3.5\times10^4$ N/m
Vertical stiffness of secondary suspension	$K_{sz} = 3.5\times10^5$ N/m
Longitudinal damping of secondary suspension	$C_{sx} = 3.2\times10^4$ N-s/m
Lateral damping of secondary suspension	$C_{sy} = 1\times10^4$ N-s/m
Vertical damping of secondary suspension	$C_{sz} = 4\times10^4$ N-s/m

Wind loads:

Parameters	Value
Length of car body	$L = 26.2$ m
Width of car body along the mean wind flow	$B = 3.38$ m
Height of car body normal to the main stream direction	$H = 3.84$ m

鐵路車輛在風力作用下的脫軌風險分析

鄭永長　　陳振華　　葉崇偉

國立高雄科技大學機電工程學系

國立高雄大學土木與環境工程學系

國立空軍航空技術學院飛機工程系

摘 要

本文旨在探討鐵路車輛在承受軌道不整與風力作用下的脫軌風險分析。考慮非線性的輪軌接觸力，建立 31 個自由度的鐵路車輛模型與運動方程式。依據脫軌準則，分別計算脫軌係數、輪重減載係數以及傾覆係數。由分析結果顯示，脫軌係數、輪重減載係數以及傾覆係數隨著風力的攻角增加而升高。而且，根據線性與非線性輪軌接觸力的比較分析，以非線性接觸力計算得到，可得到較高的脫軌係數、輪重減載係數以及傾覆係數。總而言之，風力的攻擊角對於鐵路車輛的脫軌風險有重大的影響。